A New Model of Solar Ultraviolet Irradiance Variability with 0.1-0.5 nm Spectral Resolution

Lean Judith L.[1], Coddington O[1], Marchenko S V[2], and Deland M T[2]

[1]University of Colorado
[2]Science Systems and Applications

November 16, 2022

Abstract

Key Points * NRLSSI2h solar irradiance variability model with 0.1-0.5 nm resolution captures larger UV. spectral line variability relative to continua. * At 300-400 nm, dominated by spectral features, NRLSSI2h estimates 2-5X smaller solar cycle variability than radiative transfer models. * Upper atmosphere solar radiation absorption can differ using NRLSSI2h (e.g., 34% decrease at 88 km for Lyman alpha).

A New Model of Solar Ultraviolet Irradiance Variability with 0.1-0.5 nm Spectral Resolution

J. L. Lean[1], O. Coddington[1], S. V. Marchenko[2], M. T. DeLand[2]

1. *Laboratory for Atmospheric and Space Physics, University of Colorado, Boulder, CO 80305*

2. *Science Systems and Applications, Inc., Lanham, MD 20706*

Key Points

- NRLSSI2h solar irradiance variability model with 0.1-0.5 nm resolution captures larger UV. spectral line variability relative to continua.
- At 300-400 nm, dominated by spectral features, NRLSSI2h estimates 2-5X smaller solar cycle variability than radiative transfer models.
- Upper atmosphere solar radiation absorption can differ using NRLSSI2h (e.g., 34% decrease at 88 km for Lyman alpha).

Abstract

Observations of solar irradiance made from space since 2003 with 0.1 nm spectral resolution at wavelengths from 115 to 310 nm and 0.5 nm spectral resolution at wavelengths from 260 to 500 nm are used to construct a new model, NRLSSI2h, of solar irradiance variability with higher spectral resolution than the 1 nm NRLSSI2 model used to specify the NOAA Solar Irradiance Climate Data Record. The new model better resolves irradiance variability in specific emission and absorption features that are directly attributable to atoms and molecules in the Sun's atmosphere. Singularly prominent is spectral irradiance variability at 379 to 389 nm, dominated by the CN molecular band system; irradiance in this 10 nm band increased 0.078 W m^{-2} during solar cycle 23, contributing 4.6% of the 1.7 W m^{-2} concurrent total solar irradiance increase. Irradiance variability at wavelengths from 300-400 nm, a region dominated by multiple spectral features, is a factor of 2 to 5 smaller in the new model than estimated by semi-empirical models that use radiative transfer codes to calculate the contrasts of faculae and sunspots, which alter the temperature-dependent densities of these species relative to the surrounding continuum. Solar atmosphere temperature and composition profiles in radiative transfer models may therefore not be realistic or their atomic and molecular databases complete. Improved co-location of spectral features in solar irradiance and the absorption cross sections of molecular oxygen and ozone with the new model may allow higher fidelity calculations of energy deposition in Earth's atmosphere.

1 Introduction

Terrestrial research requires reliable knowledge of the Sun's radiative output, which is Earth's primary energy source. Changes in this output may alter terrestrial radiative, chemical and dynamical processes on time scales of the Sun's 11-year activity cycle and longer, producing natural changes in the coupled Earth system (e.g., Lean, 2017). Solar ultraviolet radiation, in particular, is a primary determinant of the state of Earth's atmosphere, including the ozone layer. Physical simulations and empirical analyses of geophysical climate and ozone chemistry and dynamics input solar spectral irradiance variability to separate natural and anthropogenic components. NOAA established, and maintains for use by Earth scientists, the Solar Irradiance Climate Data Record (CDR) which utilizes the Naval Research Laboratory Solar Spectral Irradiance (NRLSSI2) model to specify daily solar spectral irradiance daily at wavelengths from 115 to 100,000 nm (Coddington & Lean, 2015; Coddington et al., 2016; Coddington et al., 2019).

The Sun's radiation spectrum is a complex mix of absorption and emission features superimposed on continua emission. Solar atmosphere temperature determines the continuum spectrum and the impedance of this emission by atoms and molecules in the solar atmosphere produce the absorption and emission spectral features. Figure 1 shows the solar spectral irradiance at 0.1 nm resolution during 2009, a time of low solar activity, compared with the radiation spectra of black bodies at temperatures of 4470 and 5990 K, a temperature range that encompasses the ultraviolet and visible irradiance spectrum. Middle ultraviolet radiation (200-300 nm), near ultraviolet radiation (300-400 nm), visible and longwave infrared radiation are formed in the photosphere, the approximately 300 km thick lowest layer of the solar atmosphere, whereas far ultraviolet radiation (100-200 nm) emerges mainly from somewhat higher and cooler layers of the lower solar chromosphere, above which the temperature of the solar atmosphere increases with altitude (e.g., Cox et al., 1991). In the far ultraviolet spectrum (115 – 200 nm) the α line of the Lyman series of atomic hydrogen, H I Lyman α, at 121.567 nm in Figure 1a exemplifies the enhancement of continuum radiation by solar atmosphere species emission. In the middle (200-300 nm) and near (300-400 nm) ultraviolet and visible (400-750 nm) spectrum, especially at wavelengths from 250 to 450 nm, multiple solar atmospheric species absorb the continuum radiation, resulting in "line blanketing" that depresses the net solar radiative output. The Mg II h-k doublet (280.365 nm and 279.65 nm), and Ca II H-K doublet (396.847 and 393.366 nm) in Figure 1a are examples of prominent "Fraunhofer" absorption features, named for Joseph von Fraunhofer who mapped over 570 dark lines in the continuum solar spectrum caused by photon absorption by chemical elements in the solar atmosphere.

Solar emission and absorption features are more variable than the continuum emission. This is because the densities of atoms and molecules in the Sun's atmosphere that produce these features are temperature-dependent, and faculae and sunspots, the primary sources of irradiance variability, are respectively warmer and cooler than the "quiet" solar atmosphere. However, semi-empirical models that use theoretical stellar atmosphere radiative transfer codes to specify the contrasts of faculae and sunspots relative to the quiet atmosphere calculate solar ultraviolet irradiance variations that differ in both magnitude and spectral structure from the variations calculated by the empirical NRLSSI2 model, which derives the facular and sunspot contrasts from direct observations. For example, in wavelength regions dominated by Fraunhofer lines the Spectral And Total Irradiance Reconstruction (SATIRE) semi-empirical model

(Krivova et al., 2010) overestimates rotational modulation relative to both independent OMI observations and the NRLSSI2 model (Marchenko et al., 2016; Coddington et al., 2019; Lean et al., 2020), suggesting that faculae and sunspots produce less irradiance variability than stellar atmosphere models currently prescribe, at times by more than 50%, in multiple Fraunhofer lines between 250 and 400 nm. In identifying such discrepancies, empirical observation-based models such as NRLSSI2, can suggest the need for alterations to the temperature and density profiles of the atmospheres in the stellar radiative transfer codes that the semi-empirical models use.

The significant differences among estimates of solar spectral irradiance variability by observation-based and semi-empirical models extends beyond rotational time scales to the decadal solar cycle and centennial time scales. Reconciling these differences is crucial because simulations of climate and ozone change, including those used for the Intergovernmental Panel on Climate Change (IPCC, 2013) and Ozone Assessments (WMO, 2011), rely on model specifications of spectral irradiance variability to assess natural solar-forced terrestrial change (Jungclaus et al., 2017; Matthes et al., 2017). For example, one semi-empirical model estimates that spectral irradiance at wavelengths from 370 to 400 nm, dominated by the CN and Ca II Fraunhofer features, increased 3% from the seventeenth century Maunder Minimum to contemporary solar minima (Shapiro et al., 2011), 20 times more than the <0.15% increase in the NRLSSI2 historical reconstruction (Lean, 2018) based on simulations of the transport of magnetic flux in the Sun’s disk flux over this period (Wang et al., 2005). The semi-empirical model estimate is deemed too large by at least a factor of two in part because of the use of an erroneously cool model solar atmosphere (Judge et al., 2012). By better isolating the specific spectral contributions of atomic and molecular emissions, observation-based specifications of solar ultraviolet irradiance variability with spectral resolution finer than 1 nm may help expose and quantify those wavelength regions where semi-empirical models are least reliable.

Knowledge of solar ultraviolet irradiance variability with spectral resolution finer than 1 nm may also help improve understanding of the mechanisms by which solar radiation interacts with Earth's atmosphere. This is because, as Figure 1b shows, at ultraviolet wavelengths the absorption cross sections of atmospheric molecular oxygen, O_2, and ozone, O_3, which absorb essentially all of the Sun's far and middle ultraviolet radiation, have complex spectral structure superimposed on continuum features. Figure 2 shows examples of overlapping features in the solar ultraviolet spectrum and atmospheric absorption cross sections, including the approximate coincidence of the H I Lyman α peak emission at 121.567 nm with a deep minimum in the O_2 absorption cross section (Figure 2). Since the O_2 and O_3 absorption cross sections and concentrations determine the altitude at which solar ultraviolet energy is deposited in the Earth's atmosphere, errors may accrue if calculations of solar energy deposition do not fully resolve co-located spectral features in solar irradiance and atmospheric absorption cross sections.

Current models of solar spectral irradiance variability such as the NRLSSI2 model that specifies solar spectral irradiance for NOAA's CDR lack the spectral resolution needed to properly specify the complex wavelength-dependent variability of solar emission and absorption features. This paper describes a new model of solar spectral irradiance variability, NRLSSI2h, with 0.1 nm resolution at wavelengths from 115 to 310 nm, constructed from high resolution observations made by the Solar Stellar Irradiance Comparison Experiment (SOLSTICE) on the Solar Radiation and Climate Experiment (SORCE) spacecraft, and with ~0.5 nm resolution at wavelengths from 310 to 500 nm, constructed from observations made by the Ozone Monitoring Instrument (OMI) on the Aura spacecraft. The absolute scale and variability of NRLSSI2h summed into 1 nm bins are equivalent to those of the NRLSSI2 model, so that the new high-resolution model directly augments the Solar Spectral Irradiance CDR.

2 Observations

Solar ultraviolet irradiance has been observed from space since 1980 (e.g., Rottman, 2006). In particular, the SOLSTICE onboard SORCE measured far and middle ultraviolet spectral irradiance (115 to 310 nm) from 2003 to 2020 and OMI onboard AURA has measured the spectral irradiance from 265 to 500 nm since 2004 (Snow et al., 2012; Marchenko et al., 2019). The solar spectral irradiance observations made by SOLSTICE and OMI are reported in 1 nm wavelength bins, which is the native resolution of instruments on the prior Solar Mesosphere Explorer (SME) and Upper Atmosphere Research Satellite (UARS). Historically, a spectral resolution of 1 nm was considered adequate for providing the needed long-term repeatability for assessing terrestrial impacts of solar variability; an observation's measurement repeatability is generally considered to increase as the wavelength band broadens, although broad bands can obscure spectrally dependent drift errors. Observations of total solar irradiance have no spectral resolution but maximum long-term repeatability.

Both SOLSTICE and OMI actually measure solar ultraviolet radiative output with spectral resolution finer than 1 nm, thereby better resolving the multiple emission and absorption features in the solar ultraviolet spectrum but, arguably, at the expense of repeatability. Both the SOLSTICE and OMI "native resolution" observational databases, at 0.1 and 0.4-0.6 nm spectral resolution respectively, are now of sufficient duration and maturity to facilitate the investigation and modelling of solar spectral irradiance variability at spectral resolution finer than 1 nm. The solar spectral irradiance during solar minimum 2009 shown in Figure 1a is the average of spectra measured from 2009.0 to 2009.2 by SOLSTICE at wavelengths from 115 to 310 nm with 0.1 nm spectral resolution (on a 0.025 nm grid), and by OMI at wavelengths from 265 to 500 nm with spectral resolution of ~0.5 nm (on a 0.1 nm grid at wavelengths longer than 310 nm).

3 Model

The primary cause of variability in observed solar irradiance is the occurrence on the Sun's disk of bright faculae, where local emission is enhanced, and dark sunspots, where local emission is depleted. The NRLSSI2 model calculates the solar spectral irradiance, $I_{mod}(\lambda,t)$, at wavelength, λ, and time, t, as the net sum of these two competing effects;

$$I_{mod}(\lambda,t) = I_Q(\lambda) + \Delta I_F(\lambda,t) + \Delta I_S(\lambda,t) \quad (1)$$

where $\Delta I_F(\lambda,t)$ and $\Delta I_S(\lambda,t)$ are the wavelength-dependent amounts that faculae and sunspots alter a reference irradiance spectrum, $I_Q(\lambda)$, termed the "quiet" Sun, when these features are absent. As Coddington et al. (2016, 2019) and Lean et al. (2020) describe in detail, the NRLSSI2 CDR model was constructed by regressing SORCE SSI observations made from 2003 to 2015 in 1 nm bins against observed facular and sunspot proxies to establish the model coefficients. The facular brightening component is the Mg II irradiance index, $M(t)$, which is the ratio of the Mg II emission in the Fraunhofer h-k line cores to that in the wings (Skupin et al., 2004; DeLand & Marchenko, 2013), and the sunspot darkening component, $S(t)$, is calculated from direct measurements made by the Air Force Solar Observing Optical Network (SOON) sites of the area, A_s, and heliographic location, μ, of N_{spot} individual sunspots present on the solar disk at time t, allowing for the center-to-limb variation of the radiance.

The new observation-based model of spectral irradiance at higher resolution, designated NRLSSI2h, that this paper describes is constructed following the approach used to formulate NRLSSI2 but with the model coefficients determined using SOLSTICE observations from 2003.18 to 2020.16 (V18, with 0.1 nm resolution at wavelengths from 115.0125 to 309.9875 nm on a 0.025 nm grid) and OMI observations from 2006.5 to 2019.9 (with 0.6 nm resolution at wavelengths from 265.05 to 309.65 nm on a 0.2 nm grid and 0.4-0.6 nm resolution at wavelengths from 310.1 to 499.9 nm on a 0.1 nm grid). As with the construction of the NRLSSI2 1 nm model, prior to regression the irradiance observations and the facular and sunspot indices are detrended (by subtracting 81-day running means) to isolate changes during the Sun's 27-day rotation, a period sufficiently short for instrumental changes to be deemed minimal. The observed, detrended rotational modulation of solar spectral irradiance, $I_{obs}\,(\lambda,t) - \langle I_{obs}(\lambda,t)\rangle_{81}$, at wavelength, λ, and time, t, is represented by the model, $I_{mod}^{rot}(\lambda,t)$, in terms of the corresponding detrended facular and sunspot darkening indices, $Mg(t) - \langle Mg(t)\rangle_{81}$ and $S(t) - \langle S(t)\rangle_{81}$, as

$$I_{obs}\,(\lambda,t) - \langle I_{obs}(\lambda,t)\rangle_{81} = I_{mod}^{rot}(\lambda,t) + R(\lambda,t) \qquad (2)$$

where

$$I_{mod}^{rot}(\lambda,t) = d_0(\lambda) + d_1(\lambda)[Mg(t) - \langle Mg(t)\rangle_{81}] + d_2(\lambda)[S(t) - \langle S(t)\rangle_{81}] \qquad (3)$$

The model coefficients, d_0, d_1 and d_2, are determined using linear regression of the detrended observations and indices to minimize the error in the residuals of the observed and modeled spectral irradiance, $R(\lambda, t)$.

An initial model of solar spectral irradiance variability at time, *t,* is then

$$I_{mod}(\lambda, t) = I_{av}(\lambda) + d_0(\lambda) + d_1(\lambda)[Mg(t) - Mg_{av}] + d_2(\lambda)[S(t) - S_{av}] \quad (4)$$

where $I_{av}(\lambda)$, Mg_{av} and S_{av} are the averages of the irradiance and indices at all available times. This model is adjusted to match the irradiance of the NRLSSI2 model by scaling its absolute values in 1 nm bins, an adjustment that ensures that the new higher resolution model, NRLSSI2h, is consistent with the absolute magnitude and variability of NRLSSI2, and thus seamlessly augments the extant NOAA Solar Irradiance CDR. Atmospheric model simulations can therefore implement NRLSSI2h without changing the overall solar energy input, which is important for evaluating the impact of revised SSI data.

Figure 3 compares the NRLSSI2h modelled variations with SOLSTICE observations at the peak emission and in the nearby continuum of spectral irradiance within the 121-122 nm (Figures 3a, 3b) and 181-182 nm (Figures 3d, 3e) wavelength bins (SOLSTICE observations are specified every 0.025 nm). Also shown, for comparison, are the corresponding NRLSSI2 and SOLSTICE irradiance in 1 nm bins (Figures 3c, 3f). During solar cycle 23 the H I Lyman α peak emission at 121.5625 (Figure 3a) increases 47% (from ~45 to 66 mW m^{-2} nm^{-1}), the continuum emission at 121.0125 (Figure 3b) increases 30% (from ~0.093 to 0.121 mW m^{-2} nm^{-1}) and the irradiance in the 1 nm band from 121 to 122 nm (Figure 3c) increases 42% (from 6.06 to 8.6 mW m^{-2} nm^{-1}).

As expected, and demonstrated in Figure 3, the magnitudes of solar cycle variability at wavelengths corresponding to the peaks of spectral emission and absorption lines in NRLSSI2h exceed that of the adjacent continuum throughout the ultraviolet spectrum. Figure 4 shows the relative changes during solar cycle 23 in the NRLSSI2h solar spectral irradiance at wavelengths from 115 to 500 nm compared with that of the 1 nm bins in NRLSSI2. The solar cycle changes in Figure 4 are determined as the percentage increase in the average spectral irradiance from 2009.0-2009.2 (solar cycle minimum) to 2001.93-2002.18 (solar cycle maximum), as in Lean et al. (2020). Table 1 lists absolute values of spectral irradiance in dominant spectral features during solar cycle minimum, solar cycle 23 maximum and solar cycle 24 maximum (2013.53-2013.78), as well as, for comparison, the corresponding total solar irradiance. Figure 5 shows how absolute changes in solar ultraviolet irradiance during solar cycle 23 manifest within the broader spectral region from 150 to 2300 nm; in Figure 5a the solar cycle changes in NRLSSI2h are determined as the difference in spectral irradiance from 17 May 2001 (solar cycle maximum) to 15 Sept 2008 (solar cycle minimum), so as to compare them explicitly with the (much larger) changes in the ultraviolet spectrum that the Solar Radiation Physical Modeling (SRPM) semi-empirical model calculates for those same days (Fontenla et al., 2015), shown in Figure 5b. In particular, SRPM's ~5x larger increase at wavelength from 250-400 nm has significant implications for ozone photochemistry.

It is well known, and evident in Table 1, that solar ultraviolet radiation contributes significantly more to the variability of total solar irradiance than it does to total solar irradiance itself (e.g., Lean, 1989). According to NRLSSI2h and NRLSSI2, near ultraviolet irradiance summed over wavelengths from 300 to 400 nm encompasses 6.8% of total solar irradiance, but its increase of 0.267 W m^{-2} in solar cycle 23 contributes 25% of the cycle 23 total solar irradiance change of 1.06 W m^{-2}. Figure 6 and the values in Table 1 show that the contribution of ultraviolet radiation to changes in total solar irradiance in the new NRLSSI2h model has a complex spectral structure dominated by prominent spectral features on both solar cycle and solar rotation time scales. In Figure 6a the solar cycle changes are determined as the difference of the yearly averages in 2008 (solar cycle minimum) and 2000 (solar cycle maximum) so as to explicitly compare them with the (larger) contribution of the ultraviolet spectrum to the change in total solar irradiance for this same time period estimated by the semi-empirical non-local thermodynamic Equilibrium Spectral SYnthesis code (NESSY) NESSY-SATIRE model (Shapiro et al., 2015), which Figure 6a also shows. The rotational changes in Figure 6b are determined, also following Shapiro et al. (2015), as the standard deviation of the residuals of the daily time series relative to 81-day smoothed time series, from 1999 to 2010 (inclusive).

Figures 5 and 6 show that the ultraviolet spectral irradiance region that contributes most to the solar cycle change in total solar irradiance in the NRLSSI2h model and both semi-empirical models, is from wavelengths 370 to 400 nm, which includes the CN molecular band system centered at ~383 nm and the Ca II H & K Fraunhofer lines at 396.8 and 393.4 nm. The increase of 0.12 W m^{-2} (0.36%) in spectral irradiance in the wavelength band 370 to 400 nm during solar cycle 23 is 11.2% of the 1.06 Wm^{-2} total solar irradiance increase over the same time, even though the absolute flux (33 W m^{-2}) is only 2.4% of total solar irradiance (1360.60 W m^{-2}), a factor of ~5 less. NRLSSI2h clearly resolves the contributions of the CN and Ca II spectral features (cycle 23 increases are respectively 0.078 W m^{-2} at 379 to 389 nm and 0.037 W m^{-2} at 391 to 397 nm, Table 1, Figure 6), whereas the NESSY-SATIRE simulations as shown in Figure 6 do not.

The spectral region that is least variable in Figures 4, 5 and 6 is at wavelengths from 450-460 nm. In NRLSSI2h the energy in this wavelength region increases 0.05 W m^{-2} during solar cycle 23 and 0.04 W m^{-2} in solar cycle 24. Neither the SRPM nor NESSY-SATIRE semi-empirical models predict this increase; the SRPM model in Figure 5 shows a decrease of ~0.002 Wm^{-2} at wavelengths near 450 nm and the NESSY-SATIRE model in Figure 6 shows essentially no change.

More generally, the spectral irradiance variability features evident in the empirical, observation-based, NRLSSI2 and NRLSSI2h models in Figure 4, 5 and 6, and listed in Table 1, identify prominent "benchmarks" that link spectral irradiance variability and its contributions to total solar irradiance variability to the changing composition of the Sun's atmosphere with solar magnetic activity. This linkage is apparent throughout the ultraviolet spectrum, not just in discrete atomic and molecular emission and absorption lines and bands, but also in other features such as the overall factor of two decrease (from 10% to 5% during solar cycle 23, Figure 4) in relative variability near the Al I ionization edge at ~207 nm and in the value and phase of the region of minimum spectral irradiance variability near 450 nm.

4 Atmospheric Attenuation

At those ultraviolet wavelengths where solar ultraviolet spectral irradiance and the absorption cross sections of atmospheric gases vary notably within a 1 nm interval, such as shown in Figure 2, it may be expected that calculations of the deposition of solar radiation in the Earth's atmosphere might differ when using 0.1 nm spectral resolution rather than 1 nm wavelength bins.

The comparison of mesospheric molecular oxygen absorption of solar H I Lyman α radiation shown in Figure 7 illustrates the differences in atmospheric attenuation determined using the spectral irradiance at 0.1 nm and 1 nm and the molecular oxygen absorption cross sections in Figure 2a. For this comparison, the attenuation is calculated at 40 wavelengths (in increments of 0.025 nm) between 121.0 and 122.0 for the NRLSSI2h model with 0.1 nm spectral resolution (blue curves) and for the NRLSSI2 model with 1 nm spectral resolution (orange curves). The molecular oxygen absorption cross sections are similar to Lewis et al. (1983) but neglect temperature dependence. Molecular oxygen atmospheric density profiles are specified for 1 Jan 2002 at 30^o latitude, 0^o longitude and noon local solar time using the NRLMSIS2 model (Emmert et al., 2020).

At altitudes above ~140 km solar radiation at 121 nm is essentially unattenuated, and the NRLSSI2h and the NRLSSI2 in Figure 7 are equal to that of the incident spectral irradiance. At decreasing altitudes, atmospheric absorption depletes the solar spectrum differently at different wavelengths, depending on the magnitude of the O_2 absorption cross section. Summing the individual attenuation profiles at the 40 wavelengths (on 0.025 nm grid between 121 and 122 nm) in Figure 7 gives the attenuation profiles of the total solar radiative energy in the 1 nm bin from 121-122 nm shown in Figure 8a, calculated using NRLSSI2h (blue curves) and NRLSSI2 (orange curves) at solar cycle maximum (solid lines) and minimum (dashed lines). At altitudes above ~84 km there is less attenuation of solar irradiance at wavelengths between 120 and 121 nm when using NRlSSI2h than when using NRLSSI2. This is evident in Figure 8b, which shows that there is 34% less attenuation (and hence less solar radiative energy deposited) at ~88 km when using NRLSSI2h instead of NRLSSI2, during both solar maximum (solid line) and minimum (dashed line) conditions. There are also modest differences in the change in atmospheric attenuation at solar maximum and minimum, shown in Figure 8c using NRLSSI2h (blue curve) and NRLSSI2 (orange curve).

5 Discussion

The new NRLSSI2h model resolves and quantifies the variability in individual emission and absorption spectral features in the Sun's ultraviolet radiative output better than does the 1 nm NRLSSI2 model. The new model may thus contribute to improved understanding of the facular and sunspot sources of spectral irradiance variability, whose contrasts depend on the solar atmospheric composition of the atomic and molecular species that produce highly structured spectral features. By improving the coincidence of spectral features of incoming solar radiation and absorption cross sections of gases in Earth's atmosphere, the new model may also contribute to more authentic calculations of atmospheric deposition of solar radiative energy and the terrestrial impacts of its variability.

5.1. Solar Irradiance Variability Models

The observation-based NRLSSI2h model prescribes solar ultraviolet spectral irradiance changes that are significantly smaller in magnitude, and differ in detailed spectral shape, than estimates made by the semi-empirical SRPM and NESSY-SATIRE models (by factors of about 5 and 2, respectively, Figures 5 and 6). Solar cycle ultraviolet spectral irradiance variability at wavelengths 300-400 nm are likely too high in the SRPM and NESSY-SATIRE models, rather than too low in the NRLSSI2h model given our understanding of uncertainties in observations and observation-based model estimates of solar cycle spectral irradiance variability, which is of order 20%, not a factor of 2 to 5. This is demonstrated by the agreement to better than 20% between the magnitude of NRLSSI2's solar cycle changes in the wavelength band 200-400 nm with the Solar Irradiance Data Exploitation (SOLID) project observation-based composites of solar spectral irradiance (Haberreiter et al., 2017), throughout solar cycles 21, 22 and 23 (Table 5, Coddington et al., 2019).

Similarly, the NESSY-SATIRE estimates of larger rotational changes than NRLSSI2h in solar ultraviolet spectral irradiance at 350-400 nm (Figure 6b) are also likely too high. The NRLSSI2h (and NRLSSI2) models are constructed specifically to match the observed rotational modulation of solar spectral irradiance, which is measured with greater certainty than are the longer-term 11-year solar cycle changes. Furthermore, comparisons with OMI observations independently validate the magnitude of NRLSSI2's rotational modulation (Coddington et al., 2019; Lean et al., 2020). Moreover, on Carrington timescales the OMI irradiances show good agreement with numerous contemporaneous space missions and composite data sets (Marchenko et al., 2016; Marchenko et al., 2019).

That near-ultraviolet solar spectral irradiance variability is likely too large in the SRPM and NESSY-SATIRE models has implications for how these semi-empirical models estimate irradiance variability at other wavelengths because the variability in the integral of the solar spectral irradiance must match the variability of total solar irradiance. Whereas the semi-empirical models predict larger spectral irradiance variability than NRLSSI2h at ultraviolet wavelengths, especially in the vicinity of major Fraunhofer features, they predict negligible or out of phase solar cycle variability near 450 nm compared with NRLSSI2h's small positive increase, and smaller or negative spectral irradiance variability at visible wavelengths from 550 to 900 nm, where the Sun's radiative output is primarily continuum emission from the lower photosphere. These systematic differences in the variability of solar emissions formed over a range of heights in the solar atmosphere suggest that the adopted theoretical temperature profiles in the semi-empirical models may not be realistic, as Judge et al. (2012) also concluded.

That the SRPM and NESSY-SATIRE models not only differ from the NRLSSI2h model but also differ significantly from each other suggests that semi-empirical models of solar spectral irradiance variability have yet to properly compute the transfer of radiation in the sun's atmosphere arising from the quantum mechanical structure of multiple atoms and molecules. Even using non-local thermodynamical equilibrium, they are not yet able to properly quantify solar atmosphere temperature and densities in faculae and sunspots with the certainty needed for reliable estimates of solar irradiance variability. The discrepancies between semi-empirical models themselves, and their differences with the NRLSSI2h and NRLSSI2 observation-based models, caution against using semi empirical model estimates of solar spectral irradiance variability to interpret changes in Earth's climate and atmosphere.

The observation-based NRLSSI2h model may help improve semi-empirical models of solar spectral irradiance variability. Comparisons of the variability estimated by the two types of models at wavelengths dominated by primary emission and absorption features (such as those listed specifically in Table 1) could help calibrate and quantify the semi-empirical model characterizations of magnetic features in the solar atmosphere and the combinations of bright faculae and dark sunspot features that they adopt. For example, the NRLSSI2h model shows that the Ca II Fraunhofer lines contribute ~50% as much as the CN molecular system to spectral irradiance variability at wavelengths from 370 to 400 nm, a region whose variability Shapiro et al. (2011, 2015) attribute primarily to CN in their NESSY-SATIRE semi-empirical model, which does not appear to adequately resolve the Ca II and CN features. Such comparisons could be particularly instructive for rotational time scale variability, on which the observation-based models are based and are therefore relatively robust, as demonstrated also by independent validation.

5.2. Solar Energy Deposition in the Atmosphere

The spectral resolution of co-located features in incident solar radiation and atmosphere absorption cross sections can affect calculations of solar energy deposition in the terrestrial atmosphere, as the attenuation of solar Lyman α radiation by molecular oxygen shown in Figures 7 and 8, demonstrates. That the peak emission at 121.567 nm coincides with a deep minimum in the O_2 absorption cross section (Figure 2) allows the more spectrally variable H I Lyman α emission to penetrate more deeply into the Earth's atmosphere than does far ultraviolet radiation in the less variable wings of the line. By better resolving the solar H I Lyman α line profile, the 0.1 nm spectral resolution NRLSSI2h model permits improved calculations of its atmospheric absorption. Since solar Lyman α radiation is a dominant source of energy for the mesosphere and water vapor dissociation, properly specifying the spectral dependence of its variability may improve simulations of solar influences on mesospheric variability.

In some wavelength regions such as 279-282 nm, where solar spectral irradiance variability is strongly wavelength dependent due to the Mg II h-k Fraunhofer lines but the ozone absorption cross section, near the peak of the Hartley band does not vary greatly, the differences in calculations of ozone absorption are not expected to differ greatly using NRLSSI2h and NRSSI2. More generally, a rigorous determination of the extent to which ultraviolet spectral emission and absorption feature affect solar energy deposition in the atmosphere requires spectral irradiance variability models with higher spectral resolution than 0.1 nm at far ultraviolet wavelengths and better than 0.5 nm at middle and near ultraviolet wavelengths. This is because the improved 0.1 nm spectral resolution of NRLSSI2h is still insufficient to resolve many ultraviolet emission lines that are optically thin, with widths of ~0.01 nm that may be co-located with O_2 discrete absorption in the Schumann Runge bands (175-205 nm). The newly constructed TSIS-1 Hybrid Solar Reference Spectrum (HSRS) affords such higher spectral resolution during solar cycle minimum in 2019 (Coddington et al., 2020). Evaluation of the improvement in the characterization of solar spectral irradiance using 0.1 nm instead of 1 nm resolution will require atmospheric models to utilize cross-section data with comparable spectral resolution.

6 Summary

A new model of solar ultraviolet spectral irradiance variability, NRlSSI2h, is constructed with 0.1 nm resolution at wavelength from 115 to 310 nm and 0.5 nm spectral resolution from 310 to 500 nm. The modelled irradiances summed into 1 nm bins have the same absolute scale and variability as the 1 nm NRLSSI2 model, and therefore directly augment the NOAA Solar Irradiance CDR. The auxiliary material provides a file of NRLSSI2h at wavelengths from 115 to 500 nm from 1978 to 2020 (inclusive). In future work, the NRLSSI2h (and NRLSSI2) spectral irradiance variability models will be converted to a new absolute irradiance scale based on recent measurements made by the Spectral Irradiance Monitor (SIM) on the Total and Spectral Solar Irradiance Sensor (TSIS) mission (Coddington et al., 2020) and improved by incorporating new TSIS SIM observations which have superior stability to SORCE SIM, especially at near infrared wavelengths.

By better resolving ultraviolet spectral emission and absorption features, the new observation-based NRLSSI2h model better captures the larger variability in these features than does the NRLSSI2 1 nm model. Compared to semi empirical models of solar spectral irradiance variability, the NRLSSI2h model estimates notably less variability, especially in prominent Fraunhofer absorption features, and has a different spectral structure than semi-empirical models estimate on time scales of both the solar cycle and, to a smaller extent, solar rotation. Since NRLSSI2h results are based on independent and well-documented SSI measurements during solar cycle 24, it is more likely that the semi-empirical models overestimate ultraviolet solar irradiance variability than the observation-based NRLSSI2h model underestimates the variability. This challenges the semi-empirical radiative transfer models to calculate their facular and sunspots components such that the resultant irradiance variability agrees with the constraints in both magnitude and spectral shape of the observation-based model estimates, especially on time scales of solar rotation for which the observations specify the changes with highest certainty.

The NRLSSI2h 0.1 nm spectral irradiance variability model can enable calculations of solar energy deposition in the Earth's atmosphere that better map incident solar radiation and its variability to the atmospheric altitude of its absorption, by better matching the spectral resolution of the features in the atmosphere gases that absorb this radiation. Incorporating a more accurate representation of both SSI variability and atmospheric response may affect the ability of atmospheric models to simulate changes in temperature and composition due to changing solar radiation. While the spectral resolution of the new irradiance variability model is not sufficient to resolve the details of oxygen absorption cross section in the Schumann Runge bands, it may nevertheless contribute some improvements in this region also; a new SCOSTEP/PRESTO program proposes to investigate the utility of the new higher resolution solar spectral irradiance model, and of the even higher resolution HSRS, for improving Solar terrestrial simulations (Coddington & Lean, 2021)

7 Acknowledgements

NASA supported the construction of the NRLSSI2h model as part of the Solar Irradiance Science Team (SIST) program.

References

Coddington, O., & Lean, J. (2015). Climate algorithm theoretical basis document: Total solar irradiance and solar spectral irradiance. NOAA CRDP-ATBD-0612, 56 pp.

Coddington, O., Lean, J. L., Pilewskie, P., Snow, M., & Lindholm, D. (2016). A solar irradiance climate data record. *BAMS*, July 2016, 1265-1282,DOI:10.1175/BAMS-D-14-00265.1

Coddington, O., Lean, J., Pilewskie, P., Snow, M., Richard, E., Kopp, G., et al. (2019). Solar Irradiance variability: comparisons of models and measurements. *Earth and Space Science*, 6. https://doi.org/10.1029/2019EA000693

Coddington, O. M., Richard, E. C., Harber, D., Pilewskie, P., Woods, T. N., Chance, K., et al. (2021). The TSIS-1 Hybrid Solar Reference Spectrum. Geophysical Research Letters, 48, e2020GL091709. https://doi.org/10.1029/2020GL091709

Coddington, O., and Lean, J. (2021), A New High Resolution Solar Spectral Irradiance Variability Model for Solar-Terrestrial Studies, SCOSTEP/PRESTO Newsletter, Vol. 27, April 2021.

Cox, A. N., W. C. Livingston, M. S. Matthews, Eds (1991), Solar Interior and Atmosphere, The University of Arizona Press, Tucson, AZ.

DeLand, M., & Marchenko, S. (2013). The solar chromospheric Ca and Mg indices from Aura OMI. Journal of geophysical research. Atmospheres, 118(8), 3415-3423, doi:10.1002/jgrd.50310.

DeLand, M. T., Floyd, L. E., Marchenko, S., & Tiruchirapalli, R. (2019). Creation of the GSFCSSI2 composite solar spectral irradiance data set. Earth and Space Science, 6, 1284– 1298. https://doi.org/10.1029/2019EA000616

Emmert, J. T., Drob, D. P., Picone, J. M., Siskind, D. E., Jones, M., Mlynczak, M. G., et al. (2020). NRLMSIS 2.0: A whole-atmosphere empirical model of temperature and neutral species densities. Earth and Space Science, 7, e2020EA001321. https://doi.org/10.1029/2020EA001321

Fontenla, J. M., Harder, J., Livingston, W., Snow, M., and Woods, T. (2011), High-resolution solar spectral irradiance from extreme ultraviolet to far infrared, J. Geophys. Res., 116, D20108, doi:10.1029/2011JD016032.

Fontenla, J. M., Stancil, P. C., Landi, E. (2015), Solar Spectral Irradiance, Solar activity, and the Near-ultra-violet, The Astrophysical Journal, Volume 809, Number 2

Haberreiter, M., Scholl, M., Dudok de Wit, T., Kretzschmar, M., Misios, S., Tourpali, K., & Schmutz, W. (2017). A new observa- tional solar irradiance composite. Journal of Geophysical Research: Space Physics, 122, 5910–5930. https://doi.org/10.1002/ 2016ja023492

Intergovernmental Panel on Climate Change Assessment Reports Five, Working Group I. (2013).

Judge, P. G., Lockwood, G. W., Radick, R. R., Henry, G. W., Shapiro, A. I., Schmutz, W., and Lindsey, C. (2012). Confronting a solar irradiance reconstruction with solar and stellar data. A&A, 544, A88, https://doi.org/10.1051/0004-6361/201218903

Jungclaus, J. H., Bard, E., Baroni, M., Braconnot, P., Cao, J., Chini, L. P., et al. (2017). The PMIP4 contribution to CMIP6 - Part 3: the Last Millennium, scientific objective and experimental design for the PMIP4 past1000 simulations. Geoscientific Model Development, 10, 4005-4033. doi:10.5194/gmd-2016-278.

Krivova, N. A., Vieira, L. E. A., & Solanki, S. K. (2010). Reconstruction of solar spectral irradiance since the Maunder minimum. J. Geophys. Res., 115, A12112, doi:10.1029/2010JA015431.

Lean, J. (1989). Contribution of ultraviolet irradiance variations to changes in the Sun's total irradiance, Science, 244, 197-200.

Lean, J. L. (2017), Sun-Climate Connections, Oxford Research Encyclopedia of Climate.

Lean, J. L. (2018). Estimating solar irradiance since 850 CE. Earth and Space Science, 5, 133– 149. https://doi.org/10.1002/2017EA000357

Lean, J. L., Coddington, O., Marchenko, S. V., Machol, J., DeLand, M. T., & Kopp, G. (2020). Solar irradiance variability: Modeling the measurements. Earth and Space Science, 7, e2019EA000645. https://doi.org/10.1029/2019EA000645

Lewis, B. R., I. M. Vardavas and J. H. Carver (1983). The Aeronomic Dissociation of Water Vapor by Solar H Lyman a Radiation, JGR, 88, A6, 4935-4940.

Marchenko, S. V. & DeLand, M. T. (2014), Solar spectral irradiance changes during cycle 24, *Astrophys. J* ., 789, 117, https://doi.org/10.1088/0004-637X/789/2/117

Marchenko, S. V., DeLand, M. T., & Lean, J. L. (2016). Solar spectral irradiance variability in cycle 24: observations and models, *J. Space Weather Space Clim*., 6, A40, https://doi.org/10.1051/swsc/2016036.

Marchenko, S. V., Woods, T.N., DeLand, M. T., Mauceri, S., Pilewskie, P., & Haberreiter, M. (2019). Improved Aura/OMI Solar Spectral Irradiance: Comparisons with Independent Datasets and Model Predictions. Earth and Space Science. https://doi.org/0.1029/2019EA000624

Matthes, K., Funke, B., Andersson, M., Barnard, L., Beer, J., et al. (2017), Solar forcing for CMIP6 (v3.2), *Geoscientific Model Development*, Katlenburg-Lindau Vol. 10, Iss. 6: 2247-2302.

Rottman, G. (2006), Measurements of total and spectral solar irradiance, *Space Sci. Rev*., 125, 39-51, DOI: 10.1007/s11214-006-9045-6.

Shapiro, A. I., Solanki, S. K., Krivova, N. A., Tagirov, R. V., and Schmutz, W. K. (2015). The role of the Fraunhofer lines in solar brightness variability. *Astronomy and Astrophysics*, 581:A116.

Shapiro. A. V., Shapiro, A. I., Gizon, L., Krivova, N. A., and Solanki, S. K. (2020). Solar-cycle irradiance variations over the last four billion years. *Astronomy and Astrophysics*, 636:A83.

Skupin, J., Weber, M., Bovensmann, H., & Burrows, J. P. (2004), The Mg II solar activity proxy indicator derived from GOME and SCIAMACHY, *Proceedings of the ENVISAT & ERS Symposium* (SP-572), ESA Publications Division.

Snow, M., McClintock, W.E., & Woods, T.N. (2010), Solar spectral irradiance variability in the ultraviolet from SORCE and UARS SOLSTICE, *Advances in Space Research*,46, 3, 296-302, https://doi.org/10.1016/j.asr.2010.03.027.

Wang, Y.-M., Lean, J. L., & Sheeley, Jr., N. R. (2005). Modeling the Sun's Magnetic Field and Irradiance Since 1713. The Astrophysical Journal, 625, 522–538, doi:10.1086/429689

World Meteorological Organization, 2011: Scientific Assessment of Ozone Depletion, Global Ozone Research and Monitoring Project – Report No. 52 Geneva, Switzerland.

Table 1. Radiative energy in selected spectral irradiance features (in W m^{-2} total for the specified wavelength interval), according to NRLSSI2h during solar minimum (2009.0-2009.2), solar cycle 23 maximum (2001.93-2002.18) and solar cycle 24 maximum (2013.53-2013.78), and the percentage increases in solar cycle 23 and 24. Also included are the corresponding values for total solar irradiance, according to the integrated NRLSSI2 CDR model.

Lower Wavelength nm	Upper Wavelength nm	Spectral Feature Identification	Solar Minimum W m^{-2}	Cycle 23 Maximum W m^{-2}	Cycle 24 Maximum W m^{-2}	Cycle 23 Increase %	Cycle 24 increase %
115.5	999,999.5	total solar irradiance	1360.572	1362.265	1361.418	0.124	0.062
120.8	121.2	continuum short of Lyman α	0.000040	0.000057	0.000047	42.4	17.5
121.4	121.8	H I Lyman α line	0.00585	0.00926	0.00724	58.3	23.7
181.2	181.5	continuum short of Si II lines	0.000523	0.000588	0.00055	12.4	5.1
181.55	181.85	Si II lines	0.00097	0.00119	0.00106	22.3	9.0
202	204	continuum short of Al I edge	0.0163	0.0177	0.0169	8.4	3.4
222	224	continuum long of Al I edge	0.106	0.110	0.108	3.5	1.4
279.5	279.75	Mg II k line	0.017	0.022	0.019	26.5	10.7
279.8	280.05	continuum between Mg II h-k	0.0156	0.016	0.0158	2.9	1.2
280.2	280.45	Mg II h line	0.0165	0.020	0.0179	20.3	8.2
360	370	continuum short of CN band system	10.987	11.015	11.001	0.26	0.13
379	389	CN band system	9.851	9.929	9.885	0.79	0.34
391	397	Ca II H-K lines	6.236	6.273	6.252	0.59	0.26
401	407	continuum long of Ca II H-K lines	10.721	10.732	10.728	0.11	0.07
425	435	CH	16.01	16.05	16.03	0.24	0.12
450	460	continuum long of CH	20.840	20.850	20.848	0.05	0.04

Figure Captions

1. Shown in a) is the Sun's spectral irradiance from 115 to 500 nm measured by SOLSTICE with 0.1 nm resolution at wavelengths below 310 nm and by OMI with 0.4-0.6 nm resolution at wavelengths 260 to 500 nm. Nominal black body irradiance curves for temperatures of 4470 K and 5990 K are also shown for reference. Shown in b) are the absorption cross sections of molecular oxygen, O_2, and ozone, O_3, the two gases in Earth's atmosphere that primarily absorb solar ultraviolet radiation.

2. Shown are examples of ultraviolet spectral regions where prominent solar spectral irradiance features, shown in a), are co-located with spectral structure in the absorption cross sections of atmospheric gases, shown in b).

3. Compared are the time series of solar ultraviolet irradiance observed by SOLSTICE with 0.1 nm spectral resolution (red dots) and modelled by NRLSSI2h (blue lines) at the wavelength of a) peak H I Lyman α line emission and b) the nearby continuum, compared with c) the irradiance in the 121-122 nm bin in the NRLSSI2 model and SOLSTICE observations. Compared in d) are the SOLSTICE observations (red dots) and NRLSSI2h model (blue lines) of irradiance at the wavelength of the peak Si II emission, in e) in the nearby continuum, and in f) in the 181-182 1nm bin of the NRLSSI2 model and SOLSTICE observations.

4. The increase in solar spectral irradiance at wavelengths from 115 to 500 nm from solar cycle minimum (average of days from 2009.0 to 2009.2) to the peak of solar cycle 23 (average of days from 2001.93-2002.18) is shown as the percentage change (relative to cycle minimum) in the higher resolution NRLSSI2h model (blue line, modeled using SOLSTICE in the 120-310

nm range, green line modelled using OMI in the 310-500 nm range) compared with the 1 nm NRLSSI2 model (orange line).

5. Shown in the upper panel, as an alternate depiction of solar cycle spectral irradiance variability, is the increase at wavelengths from 115 to 500 nm in energy units (W m^{-2} nm^{-1}) from one day during solar cycle minimum (15 Sept 2008) to one day near the maximum of solar cycle 23 (17 May 2001) in the higher resolution NRLSSI2h model (green line) compared with the 1 nm NRLSSI2 model (red line). Shown in the lower panel is the spectral irradiance increase (also in W m^{-2} nm^{-1}) for the same two days according to the semi-empirical SRPM model (Fontenla et al., 2015). Note the change in vertical scale relative to the upper panel.

6. Shown in the upper panel is a further depiction of the solar cycle increase in solar spectral irradiance at wavelengths from 115 to 500 nm, as a fraction of the contribution (in W m^{-2} nm^{-1}) to the corresponding increase in total solar irradiance (W m^{-2}) from solar cycle minimum (the average of all days in 2008) solar cycle 23 maximum (the average of all days in 2000). Compared with the estimates of the higher resolution NRLSSI2h model (blue line) and the 1 nm NRLSSI2 model (orange line) are the calculations of the semi-empirical NESSY-SATIRE model (green line, Shapiro et al., 2015). Shown in the lower panel are magnitudes of the modulation of solar spectral irradiance by the Sun's ~27-day rotation, according to NRLSSI2h (blue line), NRLSSI2 (orange line) and the NESSY-SATIRE semi-empirical model (green line); as in Shapiro et al. (2015), the magnitude of rotational modulation is determined as the standard deviation of the spectral irradiance relative to 81-day running means for 1999 to 2010 (inclusive).

7. Shown are the altitude profiles of solar spectral irradiance attenuated by atmospheric molecular oxygen absorption at 40 discrete wavelengths (in 0.025 nm increments) between 121 and 122 nm, determined using the higher resolution spectral irradiance variability model NRLSSI2h (blue lines). For comparison, also shown are the altitude profiles of atmospheric molecular oxygen absorption of solar spectral irradiance specified by the 1 nm band at 121.5 nm of NRLSSI2 (orange lines), for which the irradiance is constant across the 121-122 nm interval (and values at the 0.025 nm wavelength increments correspondingly constant).

8. The atmospheric attenuation of total solar flux at wavelengths 121-122 nm (the sum of the individual attenuation profiles in Figure 7) calculated using NRLSSI2h (blue lines) and NRLSSI2 (orange lines) are compared in the left panel during solar cycle minimum (dashed lines) and maximum (solid lines). The middle panel shows the differences between the attenuation profiles of the 121-122 nm solar radiation calculated using NRLSSI2h and NRLSSI2 during solar maximum (1 Jan 2002, solid line) and solar minimum (1 Jan 2009, dashed line). In the right panel are the differences in the attenuation profiles of the 121-122 nm solar radiation between solar maximum and minimum, calculated using NRLSSI2h (blue line) and NRLSSI2(orange line).

Figure 1

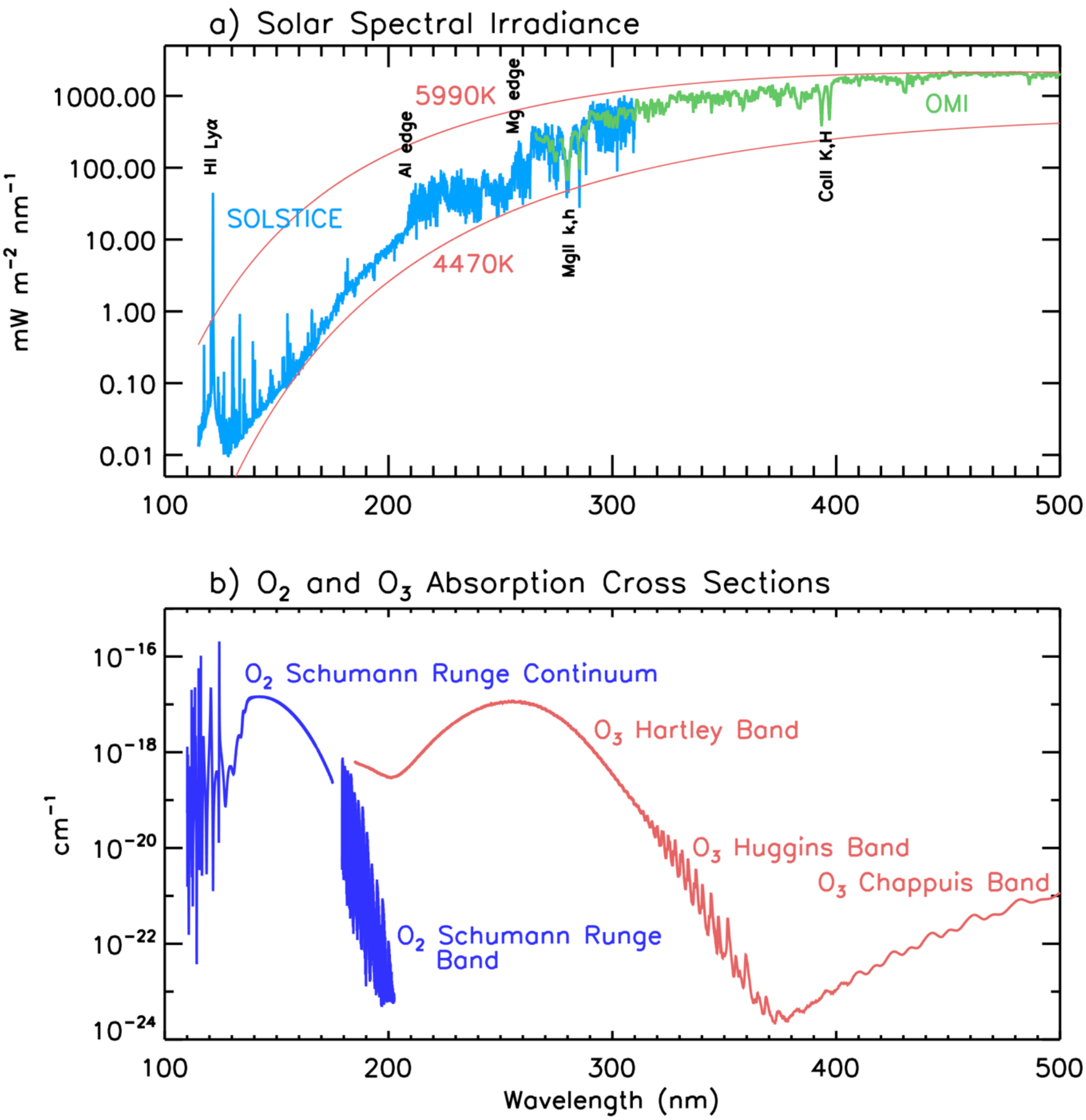
a) Solar Spectral Irradiance
mW m^{-2} nm^{-1}
1000.00
100.00
10.00
1.00
0.10
0.01
HI Lyα
SOLSTICE
5990K
4470K
Al edge
Mg edge
MgII k,h
CaII K,H
OMI
100
200
300
400
500
b) O_2 and O_3 Absorption Cross Sections
cm^{-1}
10^{-16}
10^{-18}
10^{-20}
10^{-22}
10^{-24}
O_2 Schumann Runge Continuum
O_3 Hartley Band
O_3 Huggins Band
O_3 Chappuis Band
O_2 Schumann Runge Band
Wavelength (nm)

Figure 2

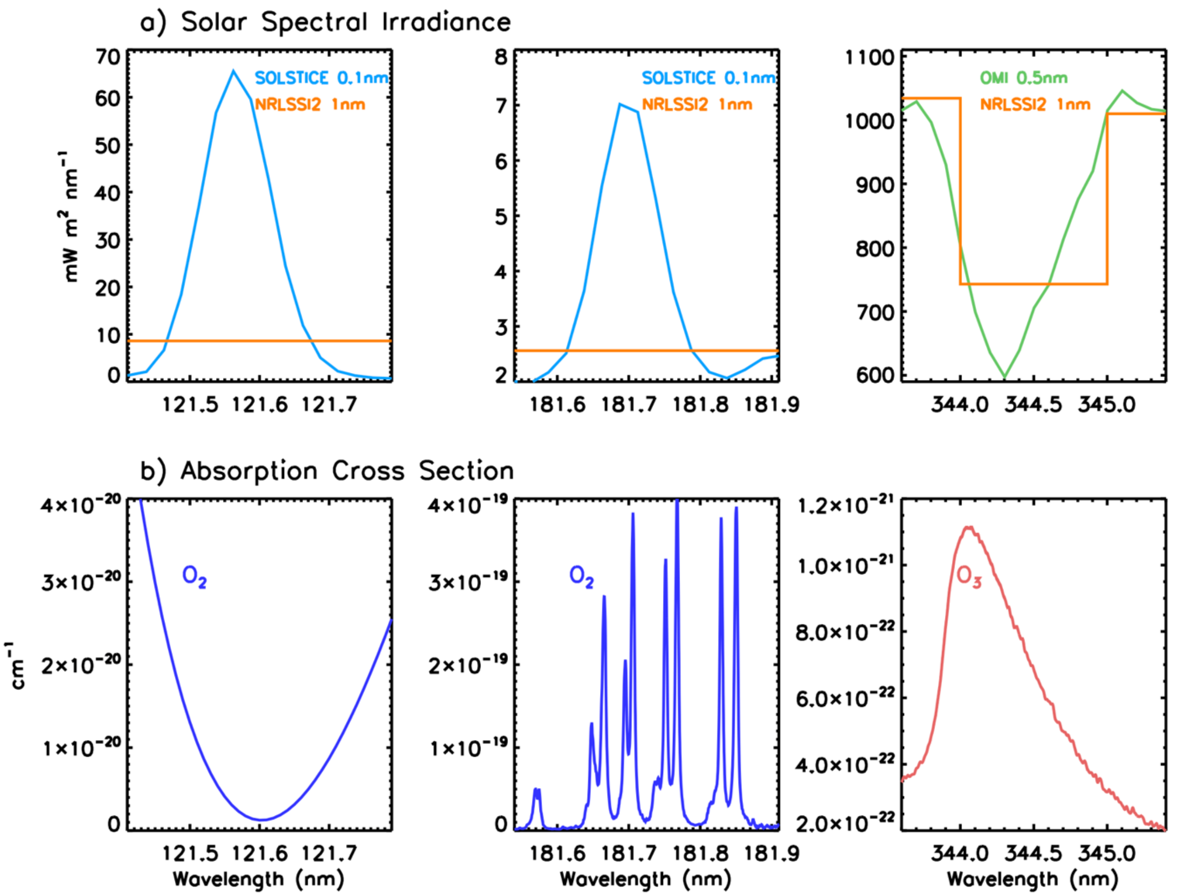
a) Solar Spectral Irradiance
mW m^2 nm^{-1}
SOLSTICE 0.1nm
NRLSSI2 1nm
70
60
50
40
30
20
10
0
121.5 121.6 121.7
SOLSTICE 0.1nm
NRLSSI2 1nm
8
7
6
5
4
3
2
181.6 181.7 181.8 181.9
OMI 0.5nm
NRLSSI2 1nm
1100
1000
900
800
700
600
344.0 344.5 345.0
b) Absorption Cross Section
cm^{-1}
4×10^{-20}
3×10^{-20}
2×10^{-20}
1×10^{-20}
0
O_2
121.5 121.6 121.7
Wavelength (nm)
4×10^{-19}
3×10^{-19}
2×10^{-19}
1×10^{-19}
0
O_2
181.6 181.7 181.8 181.9
Wavelength (nm)
1.2×10^{-21}
1.0×10^{-21}
8.0×10^{-22}
6.0×10^{-22}
4.0×10^{-22}
2.0×10^{-22}
O_3
344.0 344.5 345.0
Wavelength (nm)

Figure 3

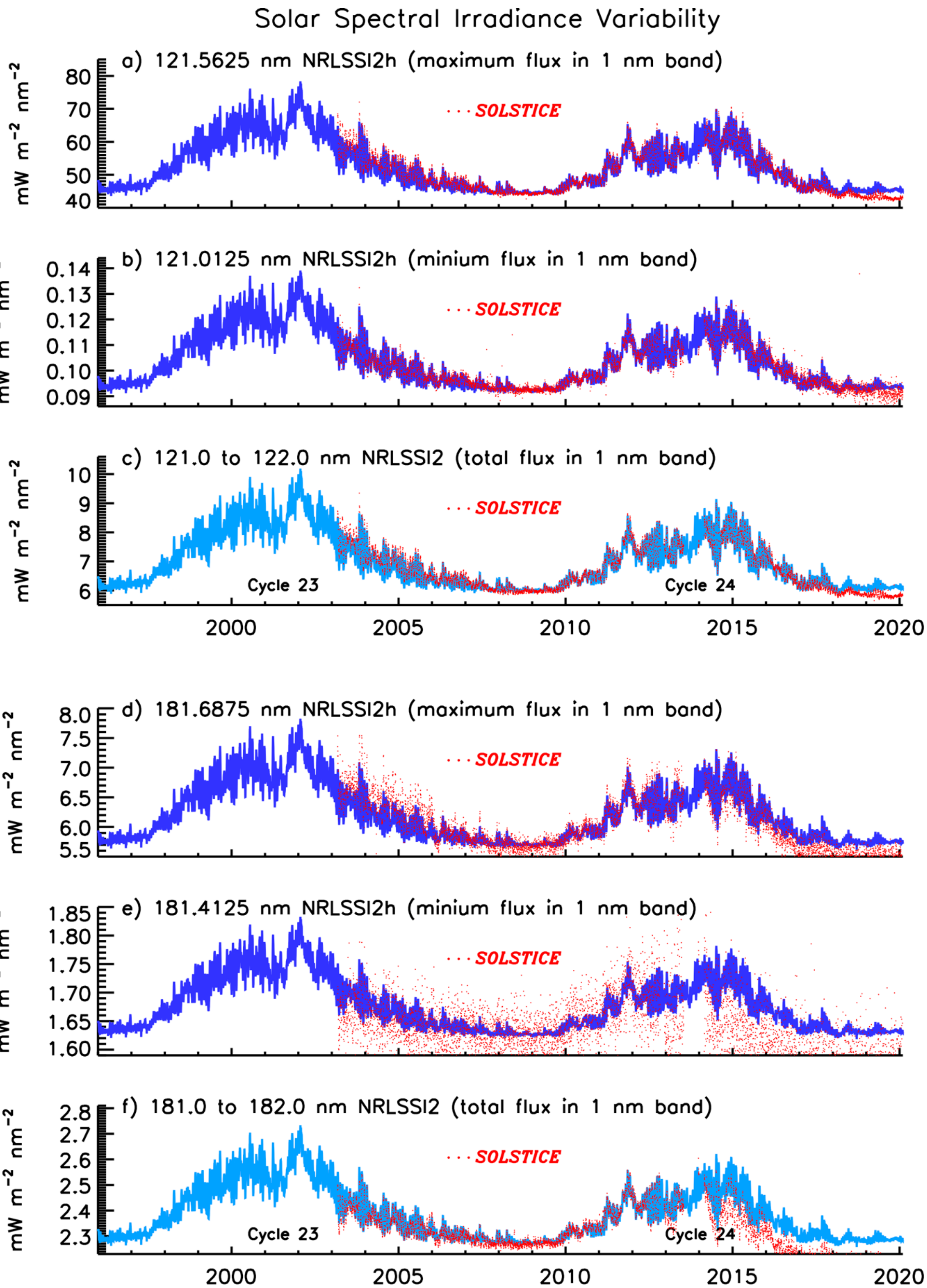

Solar Spectral Irradiance Variability
a) 121.5625 nm NRLSSI2h (maximum flux in 1 nm band)
b) 121.0125 nm NRLSSI2h (minium flux in 1 nm band)
c) 121.0 to 122.0 nm NRLSSI2 (total flux in 1 nm band)
d) 181.6875 nm NRLSSI2h (maximum flux in 1 nm band)
e) 181.4125 nm NRLSSI2h (minium flux in 1 nm band)
f) 181.0 to 182.0 nm NRLSSI2 (total flux in 1 nm band)
SOLSTICE
Cycle 23
Cycle 24
mW m^-2 nm^-2
2000
2005
2010
2015
2020

Figure 4

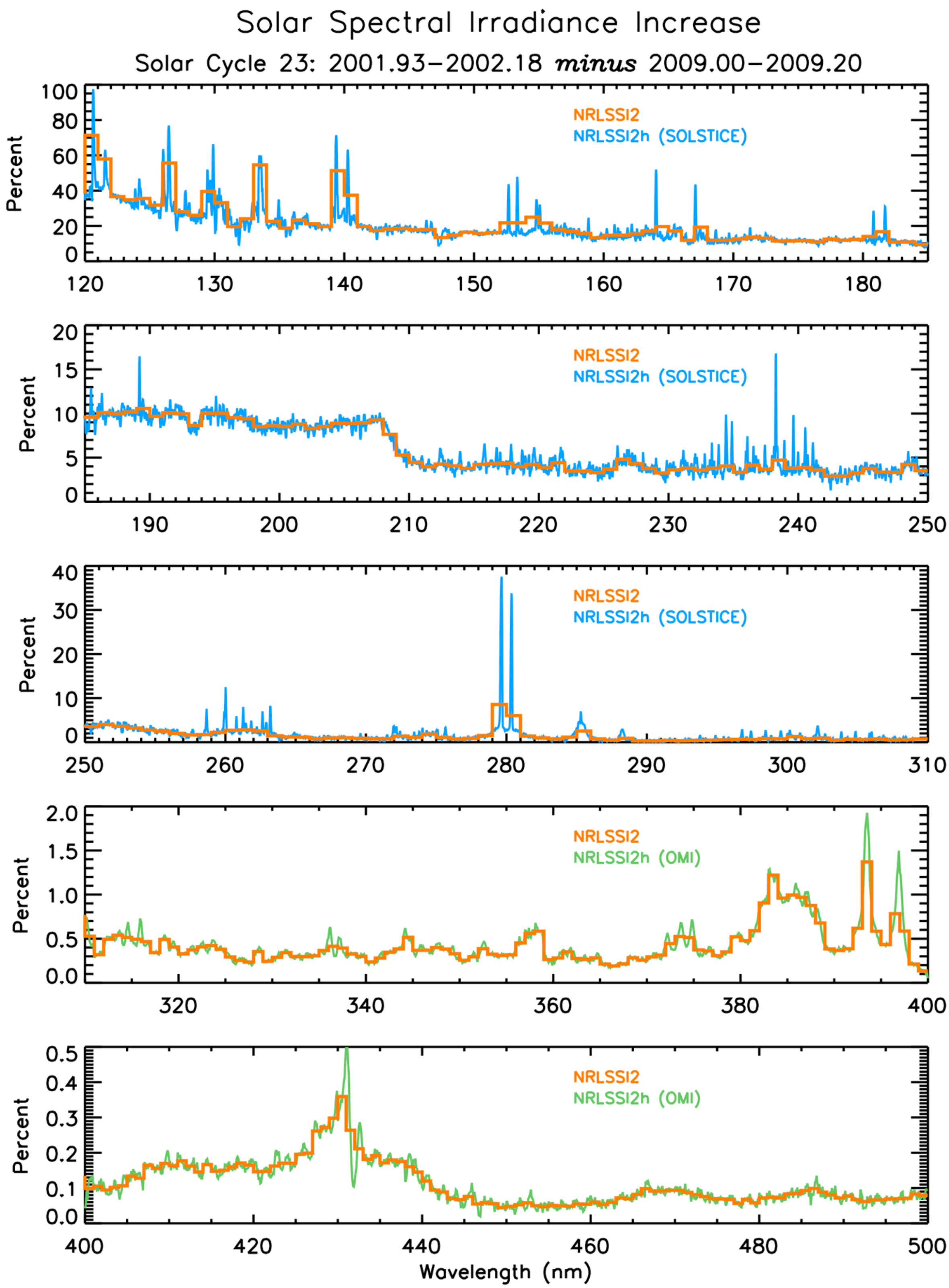
Solar Spectral Irradiance Increase
Solar Cycle 23: 2001.93–2002.18 *minus* 2009.00–2009.20
NRLSSI2
NRLSSI2h (SOLSTICE)
NRLSSI2h (OMI)
Percent
Wavelength (nm)

Figure 5

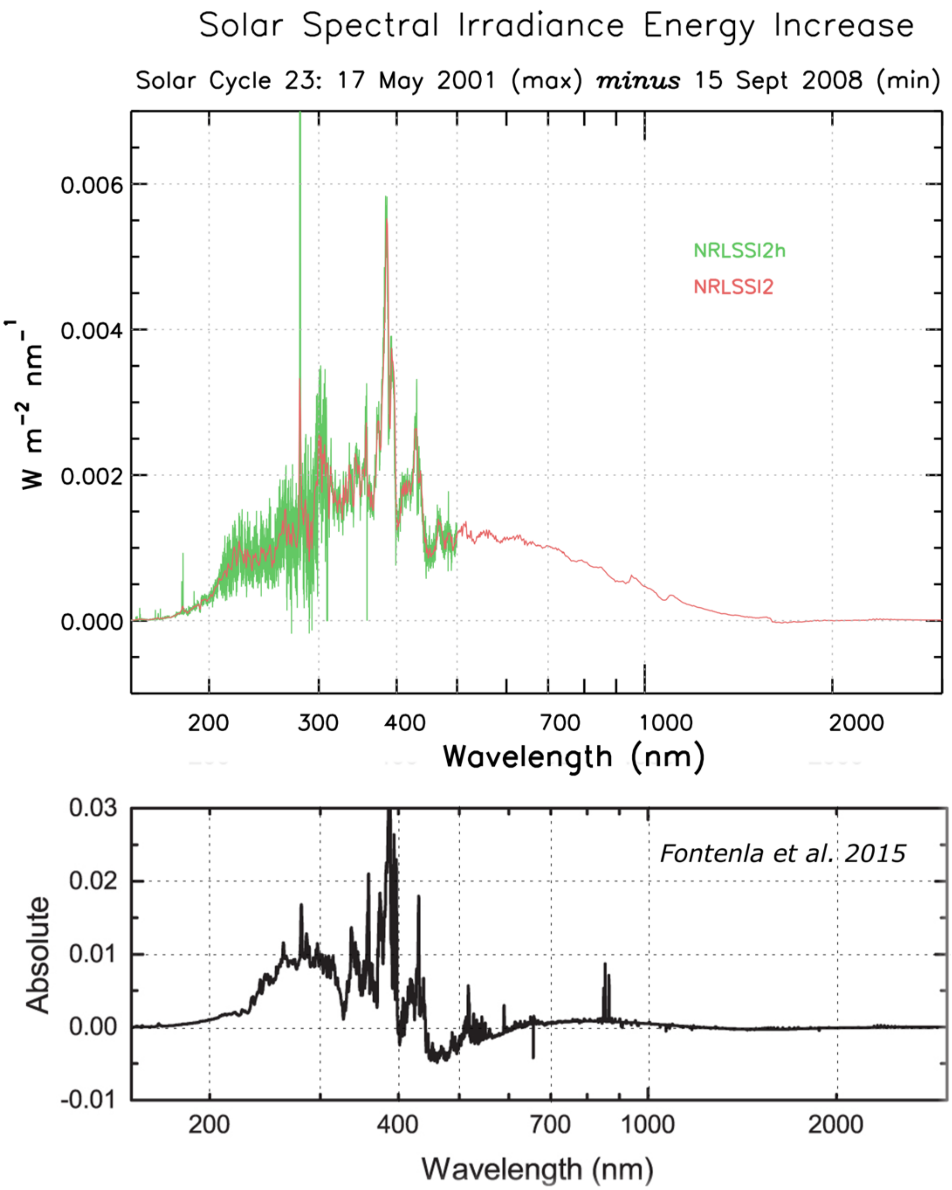

Solar Spectral Irradiance Energy Increase
Solar Cycle 23: 17 May 2001 (max) *minus* 15 Sept 2008 (min)
NRLSSI2h
NRLSSI2
W m^{-2} nm^{-1}
0.006
0.004
0.002
0.000
200
300
400
700
1000
2000
Wavelength (nm)
Fontenla et al. 2015
Absolute
0.03
0.02
0.01
0.00
-0.01
200
400
700
1000
2000
Wavelength (nm)

Figure 6

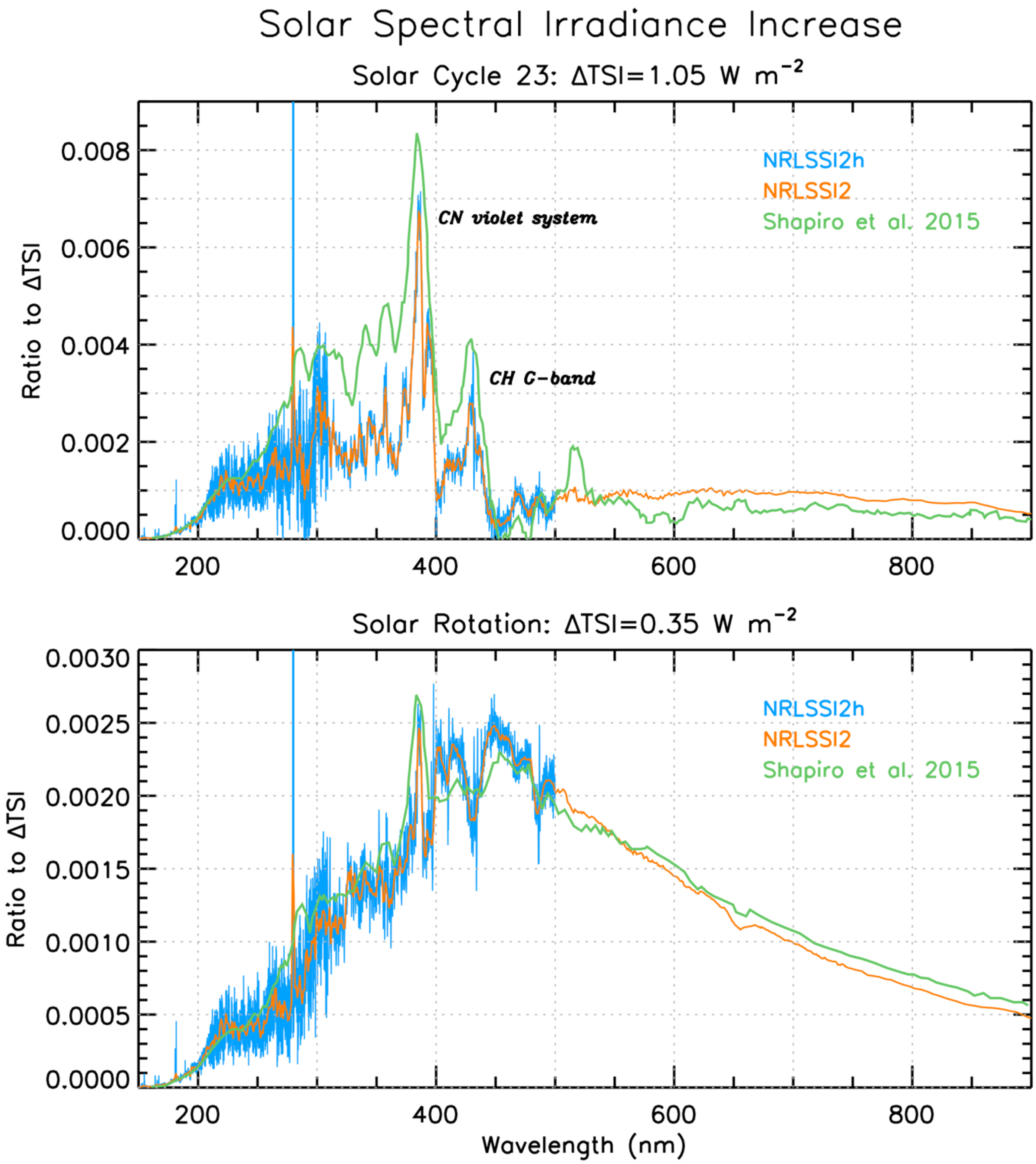

Solar Spectral Irradiance Increase
Solar Cycle 23: ΔTSI=1.05 W m⁻²
Ratio to ΔTSI
0.008
0.006
0.004
0.002
0.000
200
400
600
800
CN violet system
CH G-band
NRLSSI2h
NRLSSI2
Shapiro et al. 2015
Solar Rotation: ΔTSI=0.35 W m⁻²
Ratio to ΔTSI
0.0030
0.0025
0.0020
0.0015
0.0010
0.0005
0.0000
NRLSSI2h
NRLSSI2
Shapiro et al. 2015
Wavelength (nm)

Figure 7

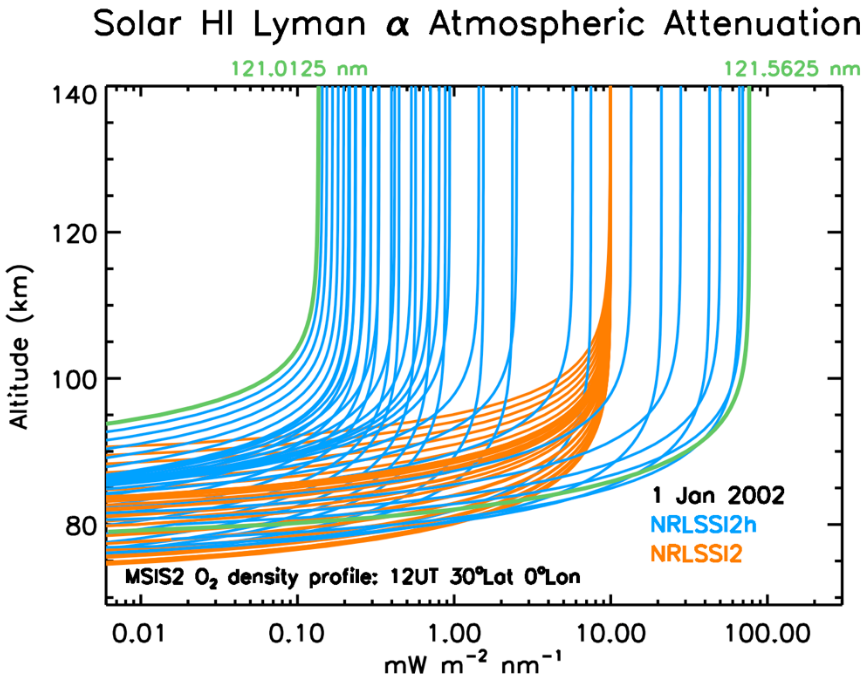
Solar HI Lyman α Atmospheric Attenuation
121.0125 nm
121.5625 nm
140
120
100
80
Altitude (km)
1 Jan 2002
NRLSSI2h
NRLSSI2
MSIS2 O2 density profile: 12UT 30°Lat 0°Lon
0.01
0.10
1.00
10.00
100.00
mW m-2 nm-1

Figure 8

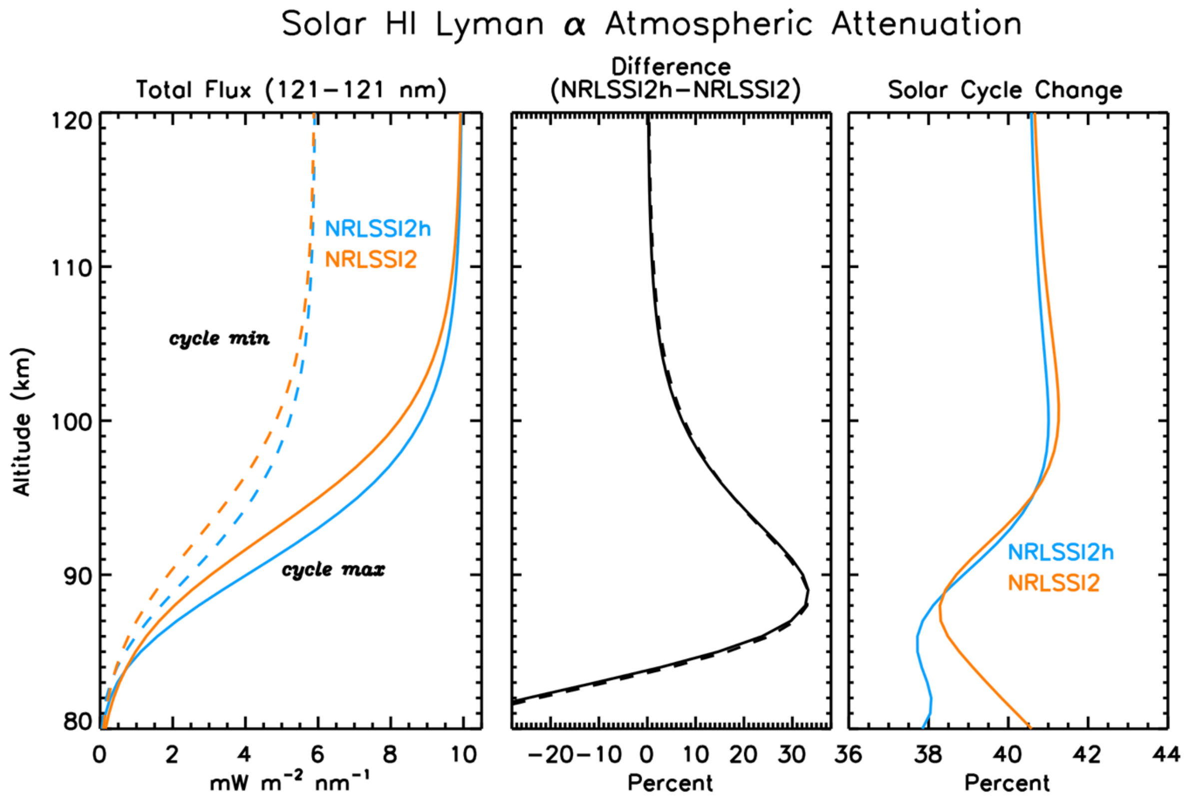

Solar HI Lyman α Atmospheric Attenuation
Total Flux (121–121 nm)
Difference
(NRLSSI2h–NRLSSI2)
Solar Cycle Change
Altitude (km)
120
110
100
90
80
NRLSSI2h
NRLSSI2
cycle min
cycle max
0
2
4
6
8
10
mW m⁻² nm⁻¹
−20
−10
0
10
20
30
Percent
36
38
40
42
44
Percent
NRLSSI2h
NRLSSI2